BJRS

BRAZILIAN JOURNAL
OF
RADIATION SCIENCES
10-03A (2022) 01-21

Effect of Mounting Orientation on Testing Equipment on Elastic Compliance of Clamped SE(T) Specimens: an exploration

Andrade[a] L.G.F., Donato[b] G.H.B., Mattar Neto[c] M.

[a, c] *Instituto de Pesquisas Energéticas e Nucleares IPEN-CNEN Av. Prof. Lineu Prestes, 2242. 05508-000, São Paulo, SP, Brazil*

[a,b] *Centro Universitário FEI. Av. Humberto de Alencar Castelo Branco, 3972-B. 09850-901, São Bernardo do Campo, SP, Brazil*

[a]*leonardogfa@gmail.com*

ABSTRACT

The accurate evaluation of fracture mechanics properties is key to the safety of operation of high responsibility structures, such as nuclear reactor components. This paper evaluates the impact of mounting orientation on the test machine of clamped *SE(T)* (*$SE(T)_c$*) specimens on their compliance. The elastic unloading compliance is a commonly used technique to measure the crack depth of specimens within fracture mechanics tests. Inaccurate measurements affect the reliability of resulting properties. Two mounting orientations are evaluated in this paper, together with two *$SE(T)_c$* specimens with different width-to-thickness ratios (*W/B=2* and *W/B=4*). The conclusions show that machine stiffness is different in the two orientations, and that this value has the potential to affect crack depth prediction. On the other hand, the analysis scope of this work was unable to detect significant differences between the two orientations, probably because loading was limited to maintain specimen integrity. Further investigation is necessary to precisely address the impact of this effect.

Keywords: **Clamped SE(T), compliance, rotation, machine stiffness.**

ISSN: 2319-0612
DOI: https://doi.org/10.15392/2319-0612.2022.1863
Submitted: 2022-01-27
Accepted: 2022-09-29

1. INTRODUCTION

The structural integrity assessment is an important task to assure the safe operation of high responsibility structures, including nuclear reactor components. This paper is part of the effort to characterize the related fracture mechanics properties that are relevant to the design and safety of operation of these structures.

1.1. Elastic unloading compliance

The Elastic Unloading Compliance technique (*EUC*) is frequently used to determine the instantaneous crack size (*a*) during fracture mechanics tests. This is based on the fact that the flexibility of the specimen increases with crack size, and that this correlation can be modeled. Other crack measuring methods, such as electric potential drop and visual inspection can also be used, but *EUC* is advantageous for the following reasons [1-3]:

1 – No additional equipment is necessary. It is based on compliance (*V/P*), which can be determined using load (*P*) and displacement (*V*). The displacement of reference is commonly the crack mouth opening displacement, *CMOD*. Both of these outputs are easily obtained using modern testing equipment with load cells and clip-gauges.

2 – Complete crack behavior through thickness. Crack depth usually varies alongside the thickness of the specimen due to changes in the stress state. The center portion tends to plane strain and the edges, to plane stress. This creates a curved crack that is deeper in the center and shallower at the edges (tunneling) and this crack profile cannot be observed with visual inspection. *EUC* is based on the elastic behavior of the entire specimen, thus capturing the effect of the whole crack. Even though tunneling is not desirable and current standards such as the *ASTM E1820* [4] limit crack curvature, several studies have been conducted to validate the *EUC* technique in predicting correct equivalent straight crack size [1].

3 – Precision. The *EUC* technique has been shown to be as precise as other available methods.

1.2. Specimen rotation and compliance

Fracture mechanics specimens are, by nature, asymmetric across their width because of the presence of a crack, where the center of the remaining ligament (W-a_0, where W is the width and a_0 is the initial crack size) is not coincident with the load line. In tension specimens, such as *C(T)*, *DC(T)*, and, the scope of this study, $SE(T)_c$, this generates uneven tensile loading in the specimen, causing a bending moment and consequent rotation [1].

Figure 1: *(a) Clamped SE(T) specimen with mounting configuration #1; (b) zoomed image; (c) Schematics; (d) zoomed image.*

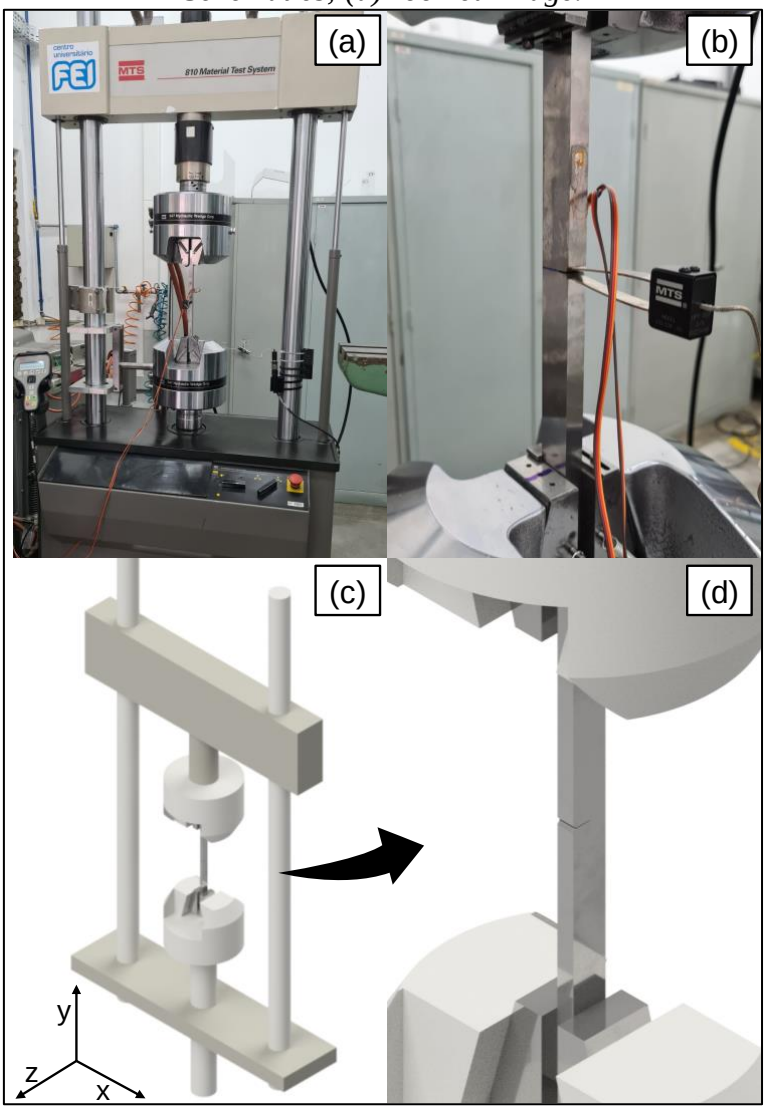

Source: Author

The traction applied to these specimens loads the remaining ligament in both traction and bending. As the loading gradually increases, the center of the remaining ligament tends to move towards the load line, decreasing the bending portion of the loading, which decreases apparent compliance [5-7].

Figure 2: *(a) Clamped SE(T) specimen with mounting configuration #2; (b) zoomed image; (c) Schematics; (d) zoomed image.*

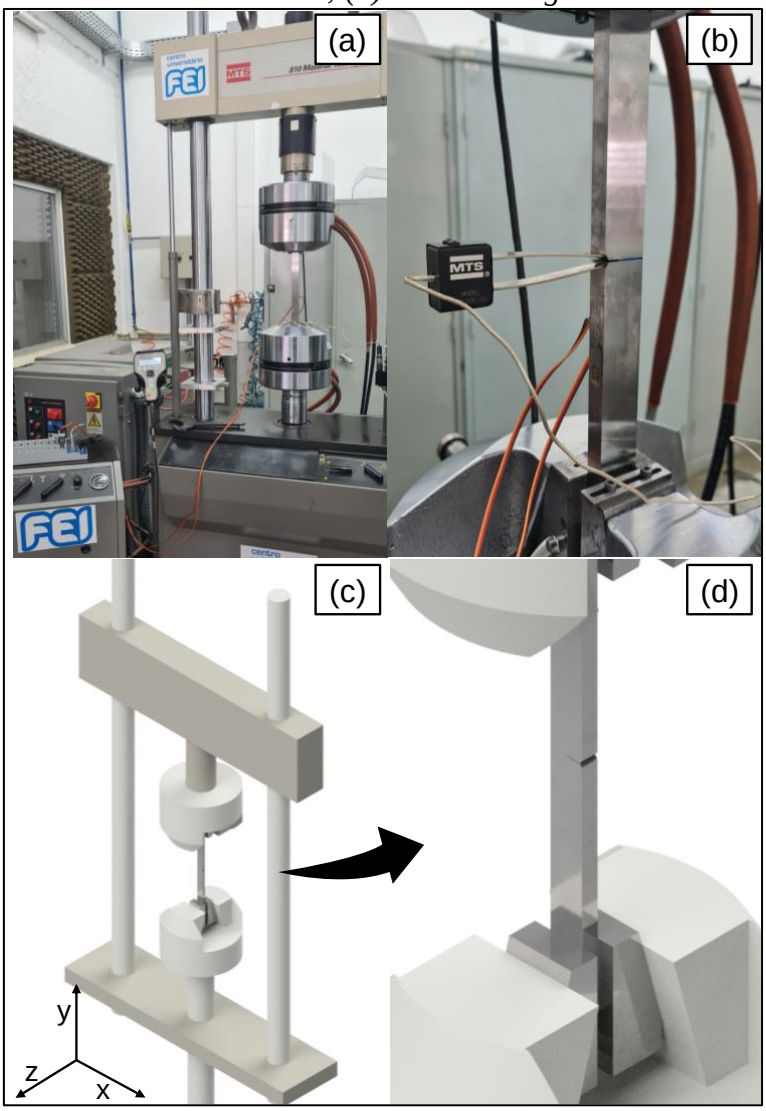

Source: Author

Although several corrections for rotation are available in the cited literature, none consider the machine frame stiffness or the rotation of the grip mechanism. This may be a problem with *SE(T)* specimens, especially the clamped ones ($SE(T)_c$), because of the mounting fixture on the test machine.

Using the coordinate system of Figure 1(c) for reference, most of the $SE(T)_c$ specimens could only be fixed on the test machine with the crack mouth pointing in the z-direction (configuration *#1*) due to grip clearance. Note that the bending moment generated by this configuration is applied across a plane with significantly less moment of inertia when compared with the crack pointing in the x-direction (configuration *#2*, Figure 2), with the grips rotated *90* degrees across the y-axis. This problem is not relevant for either of the other cited specimens because the usual mounting apparatus allows the crack to be positioned in configuration *#2*.

In this work, experimental and numerical results are conducted in a specific way in an effort to demonstrate the problem. The expected outcome is to validate the assumption that, whenever possible, the rotated position (configuration *#2,* Figure 2) should be prioritized for $SE(T)_c$ specimens.

2. MATERIALS AND METHODS

2.1. Machine stiffness estimation

For estimation purposes only, the test machine frame was roughly modeled with the specimen in both configurations using Autodesk Inventor ® [10] software. Please note that for this line of study, determination of the exact machine compliance in both directions would be ideal. Since this paper is exploratory, the authors decided to estimate the data using FEM, and if the conclusions are promising, this approach will be used. Two simple *FEM* (Finite Element Method) analyses with tetrahedral elements, linear elastic material (steel, $E = 210\ GPa$, $\nu = 0.3$), surface gluing interactions between different parts, and simplified boundary conditions (no degree of freedom allowed at the base of the machine and uniform *100 Nmm* bending moment applied in the crack tip plane nodes) were conducted to compare the impact of a bending moment applied on the x-axis and y-axis of the machine, representing, respectively, configurations *#1* and *#2*. Only the output of maximum displacement will be compared to demonstrate the stiffness difference between the configurations. All model dimensions were based on the MTS 810 universal test machine with the *SE(T)* specimen described in section 2.2 mounted. All dimensions of interest are displayed on Figure 3.

Figure 3: *Loading machine roughly modeled in CAD.*

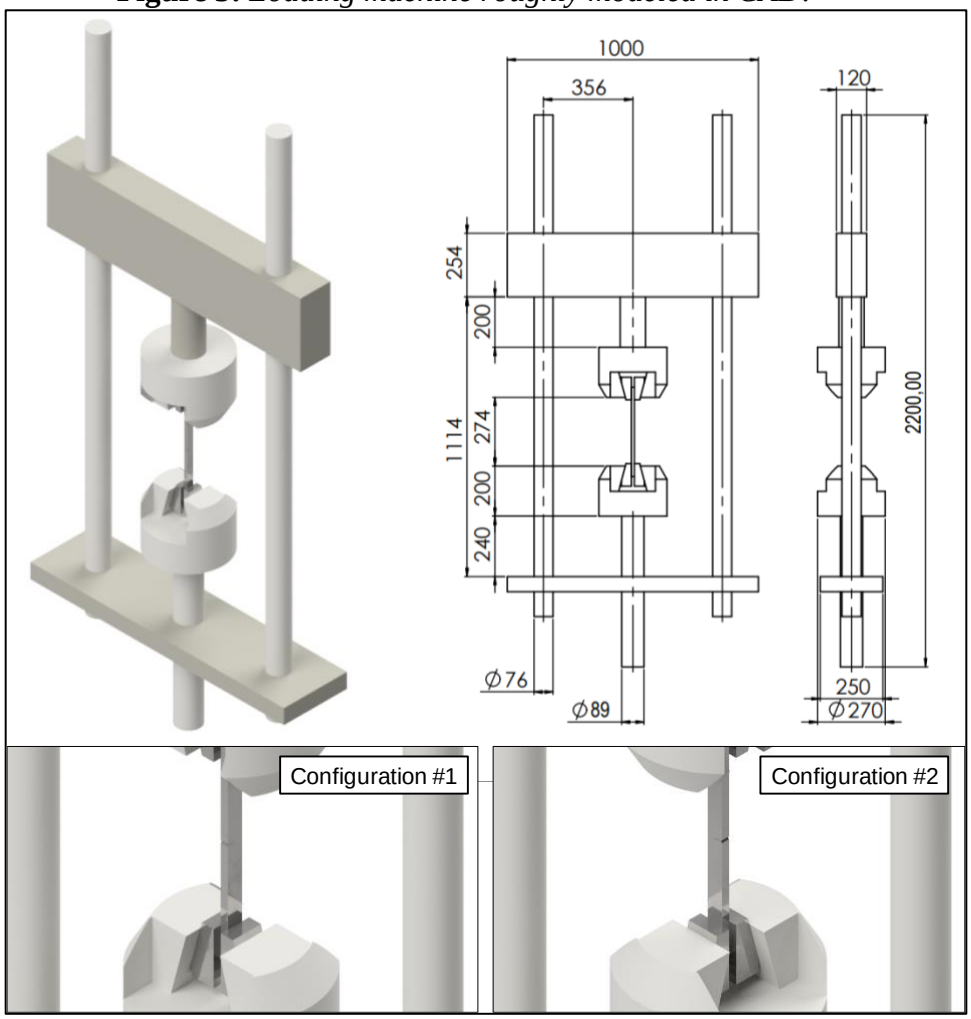

Source: Author

2.2. Mounting fixture stiffness impact on $SE(T)_c$ specimens

To demonstrate that the machine compliance has the potential to affect the apparent compliance of $SE(T)_c$, which should impact the expected outcome of the mentioned specimen and therefore the crack size prediction, *FEM* analysis of these specimens was elaborated, with special loading and boundary conditions.

The models used to reproduce the specimens are constructed in Dassault Sistèmes Abaqus® [9] software with typical symmetry conditions and a spider-web mesh crack core. Standard *8*-node hexahedral elements are used apart from the crack core, where *20*-node hexahedral second order elements are recommended to provide accurate fracture mechanics properties. The half-thickness is

discretized with *10* elements and loading is applied, with displacement in the y direction at the nodes, corresponding to the fixture in the loading mechanism (typical mesh shown in Figure 4).

The specimen model is a typical $SE(T)_c$ with the daylight length to width ratio *H/W=10* (whole length of 14W accounting for the grip area), built with a width *W=25.55 mm*, thickness *B=25.4 mm*, and relative crack depth *a/W=0.365*. To represent the effect of the machine compliance in *FEM*, the $SE(T)_c$ specimen is loaded with the scheme presented in Figure 5:

Figure 4: *Typical $SE(T)_c$ mesh.*

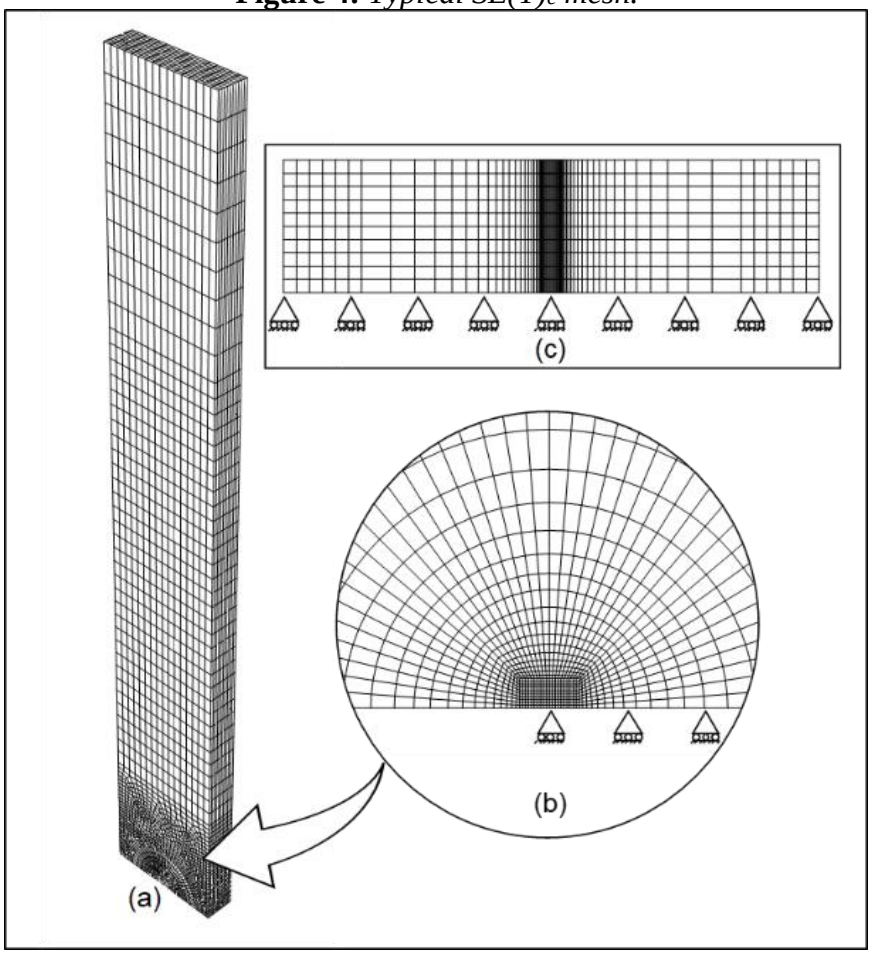

Source: Author

(a) Loading is applied via displacement (for all models, *0.5 mm* loading followed by a *0.05 mm* unloading to measure compliance). Note, that since uniform displacement is applied to the crack plane nodes, symmetry conditions are still maintained.

(b) A reference point (*RP*) is constrained to the grip area of the specimen. Only one torsional degree of freedom is allowed.

(c) Torsional spring, with configurable stiffness, joins the reference point to the ground with a torsional degree of freedom. Five values of spring stiffness are used to show the impact of this value on the compliance data.

Figure 5: *SE(T)$_c$ loading scheme.*

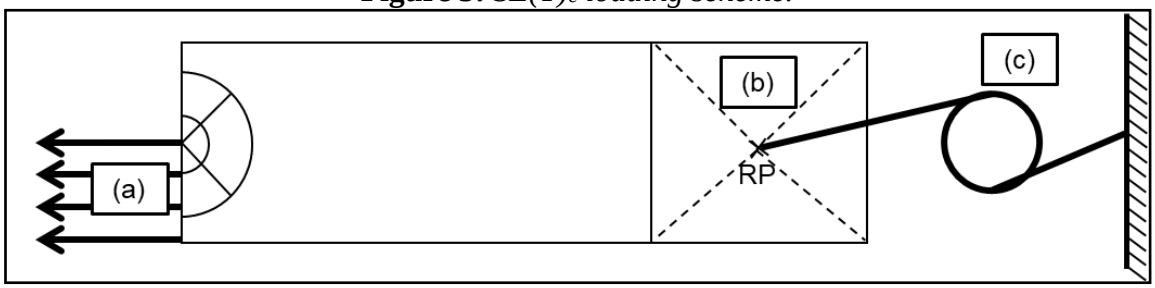

Source: Author

2.3. Experimental and numerical evaluation

SE(T)$_c$ specimens were tested in both mounting orientations following the methodology detailed below. Results were compared with *FEM* models for the complete evaluation.

Specimens were fabricated with *API 5L X65MS* [8] steel (stress-strain curve shown below in Figure 6). Two specimens were analyzed with width *W=25.4 mm* and width-to-thickness ratios of *W/B=2* and *W/B=4* respectively. The tests were conducted limiting the stress intensity factor K_I value to *25 MPa.m$^{0.5}$*, aiming to maintain minimal crack tip plasticity, which was calculated using equations *1* and *2* [6] and validated through *FEM* (Tabs. 2 and 3). This is desired so the same specimen can be evaluated in both orientations, without significant changes in geometry and residual stresses.

$$K_I = \frac{P}{B\sqrt{W}} f(a/W) \tag{1}$$

$$f(a/W) = 0.2832 + 3.8497.a/W - 1.4885.a/W^2 + 4.1716.a/W^3 + 9.9094.a/W^4 - 7.4188.a/W^5 \tag{2}$$

Both specimens were instrumented with two strain gauges (*Excel sensors*, model *PA-06-125AA-350L*, gauge factor *2*, gauge resistance *350 Ω*) in key positions, to the front and rear of the specimen, across the thickness, employing quarter-bridge configuration. Gauges were installed *2.5W* distant from the crack plane to avoid stress concentration, as shown in Figure 9. Data acquisition was performed using National Instruments ® equipment and software and gauge output voltage was converted to microstrains (*ue*), as usual.

Figure 6: *API 5L X65MS stress-strain curve.*

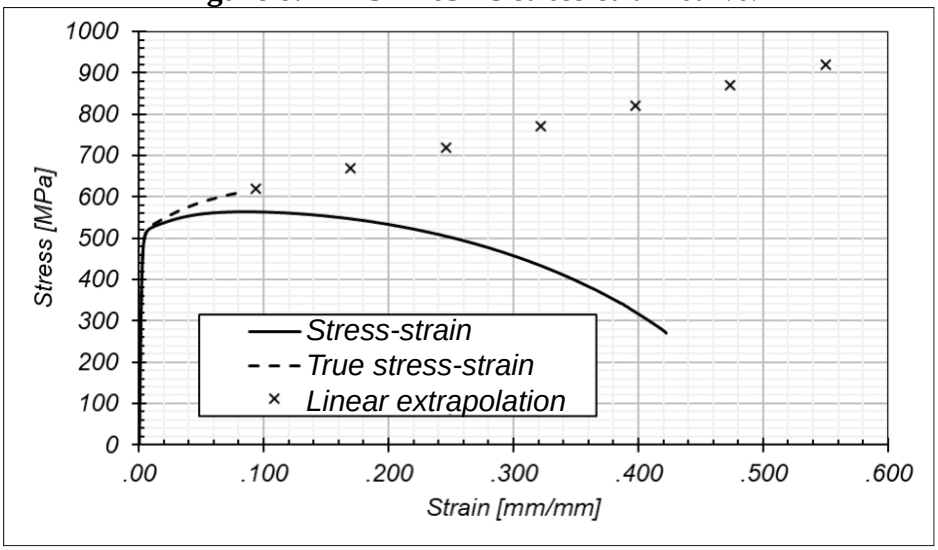

Source: Author

FEM models for both specimens (*W/B=2* and *4*) were generated, following the methodology shown in topic 2.2, apart from the spring, which was removed and the degree of freedom that it represents was fixed, turning the analysis into typical and ideal $SE(T)_c$ displacement constraints, which are basically:

(a) Restricted longitudinal displacement on the remaining ligament for symmetry;

(b) Loading is applied through the grip area via displacement and all other degrees of freedom locked. The schematics are shown in Figure 7.

Figure 7: *SE(T)c typical loading scheme.*

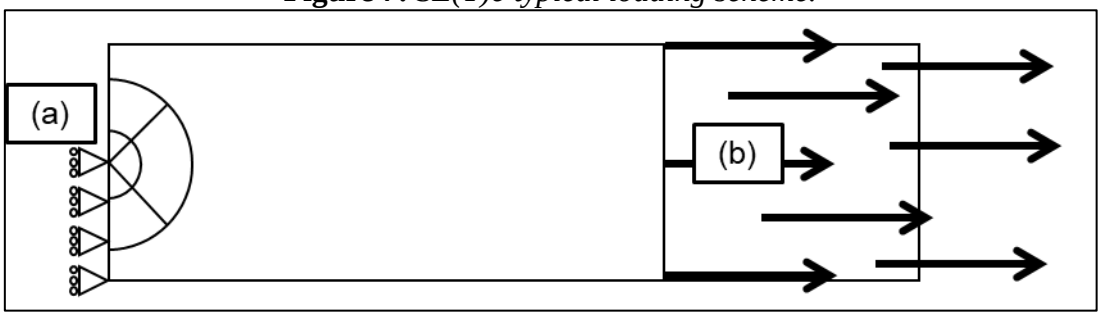

Source: Author

The data of interest extracted from the *FEM* analysis are: load, *CMOD*, rear and front gauge strains (represented by the average strains across the nodes at the distance of *2.5W* from the crack mouth), and K_I (5^{th}, 10^{th}, and 15^{th} contour). The contours are a ring of elements starting from the crack plane, with the size equivalent to the contour number; for example, the 10^{th} contour (figure 8) is a ring of 10 elements starting vertically from the 10^{th} element to the right of the crack tip and ending at the 10^{th} element to the left of the crack tip. Symmetrical constraints are considered.

Figure 8: *10^{th} contour of K_I calculation.*

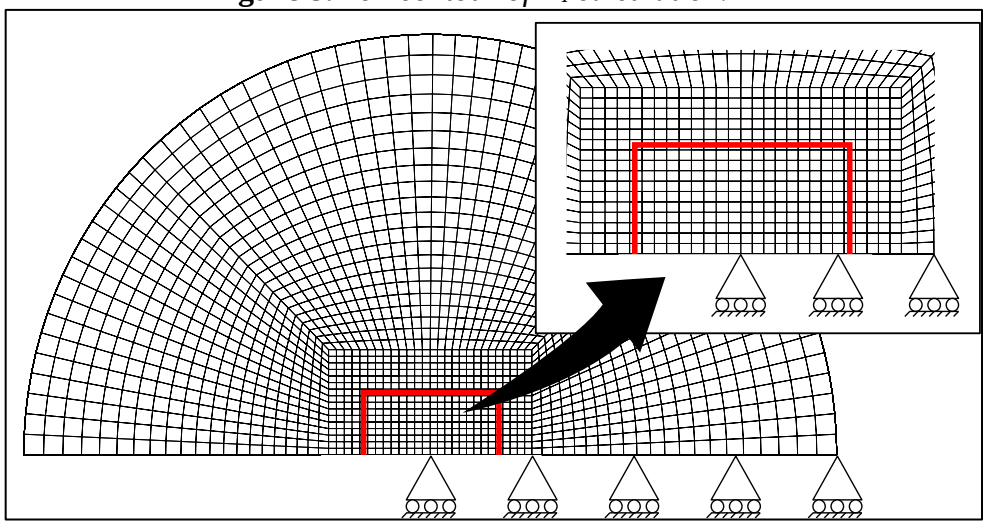

Source: Author

Since *FEM* analysis does not allow for grip rotation, it is considered to be the ideal condition. For the experimental phases, it is postulated that for equivalent load levels, all *CMOD* and gauge deformation must be equal only if no grip rotation is observed. Finally, the evaluation procedure for this work is:

1. From the *FEM* analysis, load correlations are generated as follows: load vs *CMOD*, load vs rear gauge, and load vs front gauge.
2. Experimental: load the specimen. Register *5* points equally separated up to a maximum of *25* $MPa.m^{0.5}$. For each load value, register *CMOD*, and rear gauge and front gauge deformations. Repeat *3* times and average the results.
3. Rotate the specimen along the z-axis (longitudinal rotation) in a such way that the gauges are closer to the top grip. Repeat step *2*.
4. With the correlations obtained in *1*, estimate load values for steps *2* and *3*.
5. Calculate error between estimated load and measured load.
6. Rotate the machine grips *90* degrees to achieve configuration *#2* and repeat the process.

It is expected that configuration *#2* will yield lower errors, thus being more adequate for $SE(T)_c$ tests.

Figure 9: *Strain gauges installation.*

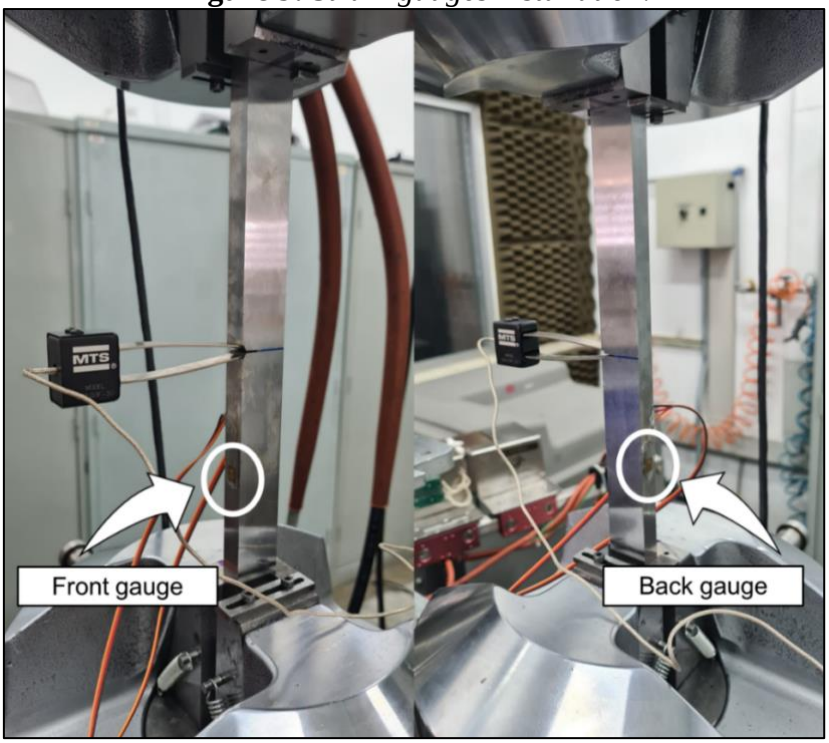

Source: Author

3. RESULTS AND DISCUSSION

3.1. Machine stiffness estimation results

Initially, the estimation of machine maximum displacement results is presented in Figure 10, conducted in Autodesk Inventor ® [10]. Please note that this does not accurately represent the test machine and should not be used quantitatively. With a uniform *100 Nmm* bending moment applied in the crack tip plane nodes, the maximum displacement in configuration *#1* was 1.9 times higher than that observed in configuration *#2*, measuring *1.877E-4 mm* versus *9.78E-5 mm*.

This confirms that the machine stiffness is different for both configurations, thus affecting the rotation of asymmetric fracture mechanics specimens, such as the $SE(T)_c$. Since rotation affects compliance, mounting orientation is potentially critical.

Figure 10: *Machine stiffness estimation results.*

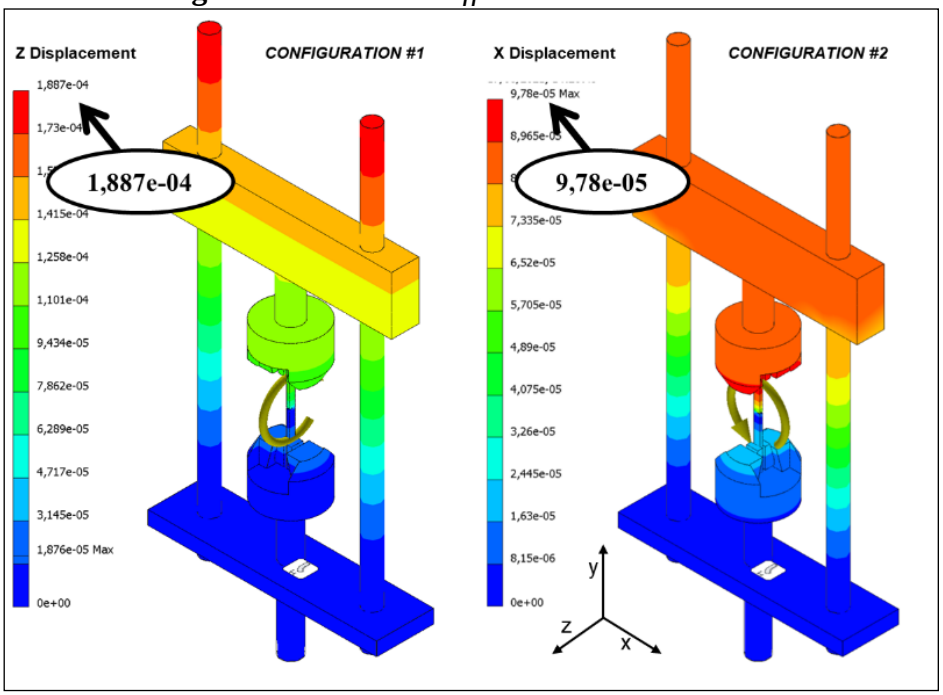

Source: Author

3.1. Mounting fixture stiffness impact on $SE(T)_c$ specimen results

$SE(T)_c$ specimen simulation results are presented in Table 1, showing spring stiffness (representing machine stiffness, *Nmm/rad*), *CMOD* (*mm*), specimen compliance (*mm/N*), and normalized compliance μ and *a/W* estimation (*mm/mm*), using Moreira's curve fitting polynomial [2]. Five arbitrary spring stiffness values with different orders of magnitude were used to verify if the machine stiffness has the potential to affect the compliance in any significant way. Note that these values are not related in any way to the values estimated previously (shown in figure 10). In future work, the determined machine stiffness values should be used instead.

Table 1: $SE(T)_c$ model simulation results.

Stiffness	***CMOD***	**Compliance**	***μ***	***a/W***
2.60E+05	1.097	1.031E-06	0.387	0.300
2.60E+06	1.049	1.108E-06	0.379	0.313
2.60E+07	0.923	1.263E-06	0.363	0.337
2.60E+08	0.870	1.288E-06	0.361	0.341
2.60E+09	0.864	1.288E-06	0.361	0.341

Table 1 confirms that the rotational stiffness of the machine has the potential to affect crack size measurement if it is low enough. Therefore, this study is relevant.

3.2. Experimental and numerical evaluation results

First, *W/B=2* numerical results are presented in Table 2. It is verified that up to *50 kN* all correlations (load vs *CMOD*, Figure 11, load vs rear gauge, Figure 12, and load vs front gauge, Figure 13) are linear. Table 3 shows the results for *W/B=4* and all the correlations are also linear, with similar behavior, and for this reason, the graphs are omitted here.

Table 2: *W/B=2 FEM* results.

Load	***CMOD***	**Rear strain**	**Front strain**	K_I, $MPa.m^{0.5}$			
N	***mm***	***mm/mm***	***mm/mm***	**5^{th} contour**	**10^{th} contour**	**15^{th} contour**	**Calculated**
0	0.0000	0.00E+00	0.00E+00	0	0	0	0
1999	0.0027	3.44E-05	2.42E-05	1.87	1.87	1.87	1.79
3998	0.0054	6.89E-05	4.85E-05	3.74	3.74	3.74	3.59
...	...	...	...	...	...	...	...
23965	0.0324	4.13E-04	2.90E-04	22.39	22.39	22.40	21.49
25956	0.0351	4.48E-04	3.14E-04	24.25	24.27	24.27	23.28
27945	0.0379	4.82E-04	3.38E-04	26.08	26.15	26.16	25.06

Figure 11: *Load vs CMOD for W/B=2, FEM result.*

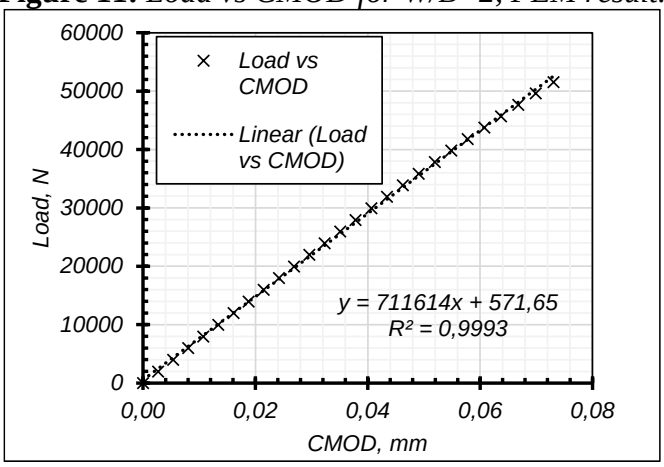

Source: Author

Figure 12: *Load vs rear strain for W/B=2, FEM result.*

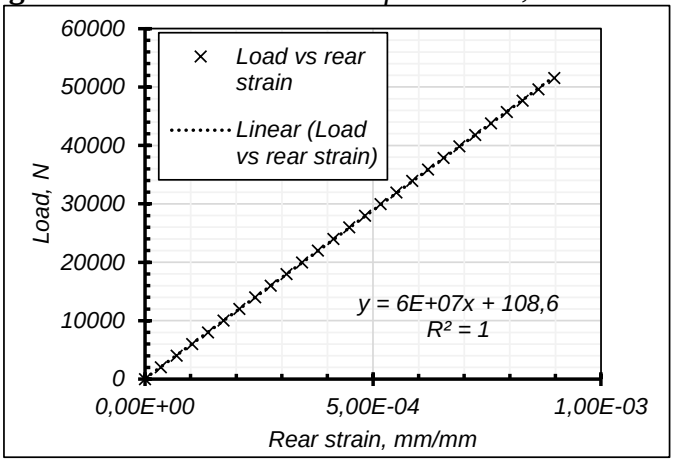

Source: Author

Figure 13: *Load vs front strain for W/B=2, FEM result.*

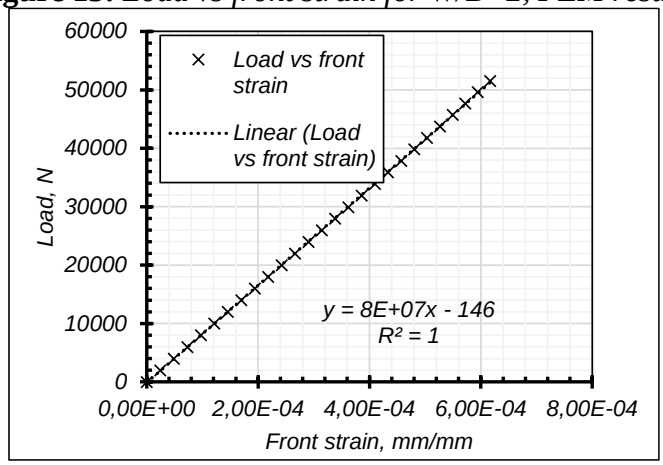

Source: Author

Table 3: *W/B=4 FEM* results.

Load	***CMOD***	**Rear strain**	**Front strain**	***K_I, MPa.m$^{0.5}$***			
N	***mm***	***mm/mm***	***mm/mm***	***5th* contour**	***10th* contour**	***15th* contour**	**Calculated**
0	0.0000	0.00E+00	0.00E+00	0	0	0	0
1015	0.0025	3.52E-05	2.55E-05	1.84	1.84	1.84	1.76
2030	0.0051	7.04E-05	5.11E-05	3.67	3.67	3.67	3.51
...	...	...	...	...	...	...	...
12167	0.0306	4.23E-04	3.06E-04	21.92	21.94	21.94	21.07
13178	0.0332	4.58E-04	3.31E-04	23.73	23.78	23.78	22.82
14188	0.0358	4.93E-04	3.56E-04	25.51	25.63	25.63	24.56

The experimental results for *W/B=2* are shown below; load vs *CMOD* in Table 4, load vs rear gauge in Table 5, and load vs front gauge in Table 6. For tables 4 to 9, errors are calculated between the corresponding load and the load cell value (*corresp.load-load cell value/load cell value*).

No significant changes were observed in the error percentage. Under lower loads, such as *5 kN*, *CMOD* error may be higher due to equipment calibration. This may indicate that in this test condition the machine stiffness is negligible.

Strain gauge results point to the same conclusion but are slightly different. For the rear gauge, the amount of error for the *1st*, *2nd*, and *3rd* measurements (gauge in top position) increases in configuration *#2*, but decreases for the *4th*, *5th*, and *6th* measurements (gauge in lower position). This may indicate that loading is not symmetrical across the crack plane of the specimen and, possibly, the center of rotation is not exactly on the crack plane. Further investigation is necessary.

Table 4: *W/B=2*, load vs *CMOD* results.

CMOD							
Measurement	**Load cell (*kN*)**	**Configuration *#1***			**Configuration *#2***		
		Clip gage (*mm*)	**Corresp. load (*kN*)**	**% Error**	**Clip gage (*mm*)**	**Corresp. load (*kN*)**	**% Error**
1st, 2nd, 3rd, average	0	0.0011	1.55	**N/A**	0.0007	1.27	**N/A**
	5	0.0064	5.24	**-4.9%**	0.0073	5.92	**-18.5%**
	10	0.0131	9.96	**0.4%**	0.0141	10.66	**-6.6%**
	15	0.0199	14.77	**1.5%**	0.0208	15.40	**-2.7%**
	20	0.0267	19.55	**2.2%**	0.0275	20.12	**-0.6%**
	25	0.0338	24.57	**1.7%**	0.0342	24.83	**0.7%**
4th, 5th, 6th (rotated longitudinally), average	0	0.0010	1.47	**N/A**	-0.0002	0.60	**N/A**
	5	0.0063	5.20	**-4.0%**	0.0065	5.34	**-6.8%**
	10	0.0131	9.98	**0.2%**	0.0134	10.17	**-1.7%**
	15	0.0201	14.89	**0.8%**	0.0202	15.00	**0.0%**
	20	0.0272	19.91	**0.5%**	0.0273	19.98	**0.1%**
	25	0.0346	25.14	**-0.6%**	0.0346	25.14	**-0.6%**

Table 5: *W/B=2*, load vs rear gauge results.

Rear Gauge							
Measurement	**Load cell (*kN*)**	**Configuration *#1***			**Configuration *#2***		
		Gauge meas. (*ue*)	**Corresp. load (*kN*)**	**% Error**	**Gauge meas. (*ue*)**	**Corresp. load (*kN*)**	**% Error**
1st, 2nd, 3rd, average	0	2	0.27	**N/A**	-12	-0.52	**N/A**
	5	82	4.83	**3.3%**	72	4.30	**14.0%**
	10	167	9.76	**2.4%**	156	9.08	**9.2%**
	15	252	14.62	**2.5%**	239	13.88	**7.5%**
	20	336	19.47	**2.7%**	323	18.69	**6.5%**
	25	419	24.21	**3.2%**	406	23.49	**6.0%**
4th, 5th, 6th (rotated longitudinally), average	0	5	0.43	**N/A**	8	0.60	**N/A**
	5	89	5.25	**-5.0%**	91	5.39	**-7.7%**
	10	172	10.02	**-0.2%**	174	10.15	**-1.5%**
	15	252	14.63	**2.5%**	255	14.79	**1.4%**
	20	330	19.11	**4.5%**	333	19.27	**3.6%**
	25	401	23.20	**7.2%**	404	23.35	**6.6%**

The front gauge conclusion is similar, but the amount of error is significantly higher. This could be an indication of strain gauge malfunction or poor gauge installation. Even though the error percentage evolution behaves similarly to the rear gauge, its results are considered inconclusive.

Table 6: *W/B=2*, load vs front gauge results.

Front Gauge							
Measurement	**Load cell (*kN*)**	**Configuration *#1***			**Configuration *#2***		
		Gauge meas. (*ue*)	**Corresp. load (*kN*)**	**% Error**	**Gauge meas. (*ue*)**	**Corresp. load (*kN*)**	**% Error**
1st, 2nd, 3rd, average	0	-2	0.04	**N/A**	11	0.76	**N/A**
	5	68	4.06	**18.7%**	77	4.58	**8.4%**
	10	133	7.78	**22.2%**	144	8.42	**15.8%**
	15	198	11.54	**23.1%**	210	12.19	**18.8%**
	20	264	15.29	**23.6%**	277	16.04	**19.8%**
	25	332	19.23	**23.1%**	343	19.88	**20.5%**
4th, 5th, 6th (rotated longitudinally), average	0	-3	-0.01	**N/A**	-4	-0.11	**N/A**
	5	63	3.76	**24.8%**	62	3.70	**26.0%**
	10	131	7.64	**23.6%**	129	7.57	**24.3%**
	15	200	11.63	**22.5%**	199	11.55	**23.0%**
	20	273	15.81	**20.9%**	270	15.65	**21.7%**
	25	352	20.36	**18.5%**	353	20.41	**18.4%**

Similar conclusions can be achieved with the *W/B=4* specimen. Load vs *CMOD* (Table 7) shows no significant changes, load vs rear gauge (Table 8) is similar to the *W/B=2* specimen, and load vs front gauge (Table 9) is also inconclusive.

Table 7: *W/B=4*, load vs *CMOD* results.

CMOD							
Measurement	**Load cell (*kN*)**	**Configuration *#1***			**Configuration *#2***		
		Clip gage (*mm*)	**Corresp. load (*kN*)**	**% Error**	**Clip gage (*mm*)**	**Corresp. load (*kN*)**	**% Error**
1st, 2nd, 3rd, average	0	0.0079	3.43	**N/A**	-0.0047	-1.27	**N/A**
	2.5	0.0041	2.02	**19.0%**	0.0055	2.52	**-0.8%**
	5	0.0110	4.60	**8.0%**	0.0122	5.02	**-0.5%**
	7.5	0.0178	7.11	**5.2%**	0.0188	7.50	**0.0%**
	10	0.0245	9.61	**3.9%**	0.0255	10.00	**0.0%**
	12.5	0.0311	12.10	**3.2%**	0.0321	12.45	**0.4%**
4th, 5th, 6th (rotated longitudinally), average	0	0.0018	1.15	**N/A**	-0.0001	0.44	**N/A**
	2.5	0.0052	2.43	**2.8%**	0.0064	2.88	**-15.3%**
	5	0.0123	5.07	**-1.5%**	0.0131	5.36	**-7.2%**
	7.5	0.0182	7.27	**3.0%**	0.0198	7.88	**-5.1%**
	10	0.0261	10.23	**-2.3%**	0.0265	10.38	**-3.8%**
	12.5	0.0330	12.79	**-2.4%**	0.0332	12.88	**-3.0%**

Table 8: *W/B=4*, load vs rear gauge results.

Rear Gauge							
Measurement	**Load cell (*kN*)**	**Configuration *#1***			**Configuration *#2***		
		Gauge meas. (*ue*)	**Corresp. load (*kN*)**	**% Error**	**Gauge meas. (*ue*)**	**Corresp. load (*kN*)**	**% Error**
1st, 2nd, 3rd, average	0	7	0.30	**N/A**	13	0.47	**N/A**
	2.5	96	2.81	**-12.5%**	103	3.02	**-20.6%**
	5	183	5.31	**-6.2%**	191	5.52	**-10.3%**
	7.5	272	7.83	**-4.4%**	280	8.05	**-7.3%**
	10	360	10.32	**-3.2%**	368	10.56	**-5.6%**
	12.5	448	12.84	**-2.7%**	459	13.16	**-5.3%**
4th, 5th, 6th (rotated longitudinally), average	0	25	0.80	**N/A**	-15	-0.35	**N/A**
	2.5	113	3.31	**-32.5%**	74	2.19	**12.2%**
	5	201	5.82	**-16.4%**	163	4.72	**5.7%**
	7.5	289	8.33	**-11.0%**	253	7.28	**3.0%**
	10	377	10.82	**-8.2%**	342	9.83	**1.7%**
	12.5	463	13.25	**-6.0%**	431	12.37	**1.0%**

Table 9: *W/B=4,* load vs front gauge results.

Front Gauge							
Measurement	**Load cell (*kN*)**	**Configuration *#1***			**Configuration *#2***		
		Gauge meas. (*ue*)	**Corresp. load (*kN*)**	**% Error**	**Gauge meas. (*ue*)**	**Corresp. load (*kN*)**	**% Error**
1st, 2nd, 3rd, average	0	-10	-0.54	**N/A**	-7	-0.42	**N/A**
	2.5	58	2.23	**10.9%**	60	2.29	**8.3%**
	5	127	5.02	**-0.5%**	129	5.08	**-1.5%**
	7.5	196	7.81	**-4.1%**	197	7.85	**-4.7%**
	10	265	10.57	**-5.7%**	266	10.62	**-6.2%**
	12.5	335	13.42	**-7.3%**	334	13.36	**-6.9%**
4th, 5th, 6th (rotated longitudinally), average	0	-21	-0.97	**N/A**	15	0.48	**N/A**
	2.5	48	1.80	**28.0%**	82	3.21	**-28.4%**
	5	116	4.56	**8.9%**	150	5.94	**-18.8%**
	7.5	185	7.35	**2.0%**	218	8.70	**-16.0%**
	10	255	10.17	**-1.7%**	286	11.43	**-14.3%**
	12.5	325	13.03	**-4.2%**	353	14.15	**-13.2%**

4. CONCLUSIONS

- The potential influence of the machine stiffness in determining the crack length of $SE(T)_c$ specimens was shown and is higher in the *XY* plane when compared with the *YZ* plane (Figure 10). This is due to the inherent design of the specimen fixture. That being said, the determination of the real machine stiffness in both configurations is mandatory for future work and definitive conclusions.
- Machine stiffness affects the results of tension specimens, exemplified by $SE(T)_c$ in this work (Table 1), and has the potential to affect accurate evaluation of fracture mechanics properties. This impact is negligible if the machine stiffness is high enough.
- In this work, load was limited to *25 kN* (*W/B=2*) and *12.5 kN* (*W/B=4*) to preserve integrity of the specimens. To date, no evidence shows that configuration *#2* should be prioritized within the limits of these loading values, and higher loading tests must be conducted to confirm the impact. Probably, tests such as *da/dN vs ΔK* might not suffer any impact of

mounting orientation because loading is lower (similar to high cycle fatigue). The problem may lie within higher loading tests such as the *J-R* test.

- Higher loading specimens and *J-R* curve characterization supported by *FEM* models with damage models are the natural next steps of this study.

SUGGESTIONS FOR FUTURE WORK

- Determine the real machine stiffness in both configurations. Use these data to feed FEM models.
- Utilize higher loading specimens and tests, such as the *1T SE(T)$_c$* (*W = 50.8 mm*) and J-R testing.

ACKNOWLEDGMENT

The authors acknowledge Centro Universitário FEI and IPEN-CNEN for the support and scholarship, which were critical for the development of this work.

REFERENCES

[1] Andrade, L. G. F.; Donato, G. H. B. Effects of crack tunneling and plasticity on the elastic unloading compliance technique for SE(B) – current limitations and proposals. **Procedia Structural Integrity**, v.13, p.1908-1914.

[2] Moreira, F. C.; Donato, G. H. B. Effects of side-grooves and 3-D geometries on compliance solutions and crack size estimations applicable to C(T), SE(B) and clamped SE(T) specimens. **Proceedings of the ASME 2013 pressure vessels & piping division**. Paris, France, 2013.

[3] Cravero, S.; Ruggieri, C. Estimation Procedure of J-resistance curves for SE(T) fracture specimens using unloading compliance. **Engineering Fracture Mechanics**, v. 74, p.2735-2757. 2007.

[4] American Society For Testing And Materials, 2018. ASTM E1820: Standard Test Method for Measurement of Fracture Toughness, Philadelphia.

[5] LOSS, F. J.; GRAY, R. A.; MENKE, B. H. J integral characterization of low upper shelf A302-B steel plate. Structural integrity of water reactor pressure boundary components. **Progress report ending 30 November 1977**, Washington, p. 18-34, May 1978.

[6] CRAVERO, S.; RUGGIERI, C. Estimation procedure of J-resistance curves for SE(T) fracture specimens using unloading compliance. **Engineering fracture mechanics**, n. 74, January 2007.

[7] SHEN, G.; TYSON, W. R. Crack size evaluation using unloading compliance in single-specimen single-edge-notched tension fracture toughness testing. **Journal of testing and evaluation**, n. 37, 2009.

[8] American Petroleum Institute, 2013. API-5L: Specification for line pipe.

[9] Dassault Systèmes Abaqus [computer software]. 2020. Retrieved from https://www.3ds.com/products-services/simulia/products/abaqus/.

[10] Autodesk Inventor [Computer software]. 2020. Retrieved from Figure 4: Machine stiffness estimation results.